nature communications

Article

https://doi.org/10.1038/s41467-025-62152-8

A mutual co-recognition mechanism ensures the proper assembly of heterotrimeric kinesin-2 for intraflagellar transport

Received: 5 February 2025

Accepted: 8 July 2025

Published online: 24 July 2025

Check for updates

Jinqi Ren[1,5], Lingyan Zhao[1,2,5], Guanghan Chen[3,5], Guangshuo Ou[3] & Wei Feng[1,4]

Heterotrimeric kinesin-2, composed of two distinct kinesin motors and a kinesin-associated protein (KAP), is essential for intraflagellar transport and ciliogenesis. KAP specifically recognizes the hetero-paired motor tails for the holoenzyme assembly, but the underlying mechanism remains unclear. Here, we determine the structure of KAP-1 in complex with the hetero-paired tails from kinesin-2 motors KLP-20 and KLP-11. KAP-1 forms an elongated super-helical structure characterized by a central groove and a C-terminal helical (CTH)-hook. The two motor tails fold together and are co-recognized by the central groove of KAP-1. The adjacent hetero-pairing trigger sequences preceding the two tails form an intertwined heterodimer, which co-captures the CTH-hook of KAP-1 to complete the holoenzyme assembly. Mutations in the interfaces between KAP-1 and the two tails disrupt the heterotrimeric kinesin-2 complex and impair kinesin-2-mediated intraflagellar transport. Thus, KAP-1 and the hetero-paired motors are mutually co-recognized, ensuring the proper assembly of heterotrimeric kinesin-2 for cargo transport.

Intracellular transport, primarily powered by cytoskeletal motor proteins, is a fundamental cellular process that dictates the delivery and distribution of various components within cells[1–3]. Kinesins are a family of microtubule-based molecular motors that utilize the energy from ATP hydrolysis to drive long-range intracellular transport[4–6]. Most of processive kinesins adopt a dimeric conformation due to a long, extended stalk formed by their internal coiled-coils, resulting in an architecture with two motor domains (or heads) that alternately bind to and move along microtubule tracks[7,8]. In addition to the two motor heads and a dimeric coiled-coil stalk, kinesin proteins possess two characteristic motor tails, which are believed to associate with cargoes for transport[4,9]. In some kinesins (such as kinesin-1 and -2), the motor tails can further recruit kinesin accessory proteins (commonly referred to as light chains) to assemble a hetero-multimeric kinesin holoenzyme, enabling more sophisticated transport functions[5,10]. Moreover, these kinesin accessory proteins serve not only as cargo adaptors but also as regulators that control motor activities, including autoinhibition and cargo-mediated activation[11].

Among transport kinesins, kinesin-2 is unique in terms of the holoenzyme assembly and can be classified into two categories based on different multimeric states: homodimeric and heterotrimeric states, primarily for intraflagellar transport and ciliogenesis[10]. Homodimeric kinesin-2 is formed by two identical motor proteins brought together by a coiled-coil stalk, resembling the structural topology adopted by the majority of kinesins, such as the heavy chains of kinesin-1[5,12]. However, in heterotrimeric kinesin-2, the holoenzyme is composed of two distinct motor proteins and an accessory protein known as kinesin-associated protein (KAP), which was originally identified through co-purification with the two motor proteins[10,13]. Although these two types of kinesin-2 motors perform

[1]State Key Laboratory of Biomacromolecules, Institute of Biophysics, Chinese Academy of Sciences, Beijing, China. [2]School of Life Sciences, Division of Life Sciences and Medicine, University of Science and Technology of China, Hefei, China. [3]School of Life Sciences, Tsinghua University, Beijing, China. [4]College of Life Sciences, University of Chinese Academy of Sciences, Beijing, China. [5]These authors contributed equally: Jinqi Ren, Lingyan Zhao, Guanghan Chen. e-mail: wfeng@ibp.ac.cn

different cellular functions in mammals[14,15], they can cooperate to control cargo import and transport in the cilia of *Caenorhabditis elegans* with an intricate handover manner[16,17]. More intriguingly, due to its asymmetric structural features, heterotrimeric kinesin-2 exhibits unusual mechanochemical properties and intrinsic capacities to move along the axoneme of cilia[18–21]. Thus, the unique components and motor properties of heterotrimeric kinesin-2 set it apart from other transport kinesins and may confer specialized motility for intraflagellar transport.

How the two distinct motor proteins can be recognized by one accessory protein KAP is intriguing and fundamental to the assembly of heterotrimeric kinesin-2. Previous studies suggest that the two motor proteins form a heterodimer via the central coiled-coil stalk, with the extreme C-terminal end likely acting as a seed to trigger their hetero-pairing (referred to as the hetero-pairing trigger sequence (HTS))[22–24]. Meanwhile, the accessory protein KAP primarily associates with the two flexible tails of the pre-assembled motor heterodimer through an unknown mechanism to assemble the heterotrimeric holoenzyme[25–27], and some studies indicate that KAP may also bind to the coiled-coil stalk of the motor proteins, further stabilizing the heterodimer[28]. More importantly, the heterodimerization of the two motor proteins appears to be a prerequisite for their association with KAP to constitute heterotrimeric kinesin-2[20], although the underlying mechanism remains to be elucidated.

In this study, we characterize heterotrimeric kinesin-2 from *Caenorhabditis elegans*, specifically the KLP-20/KLP-11/KAP-1 complex[10], and determine the structure of KAP-1 in complex with the hetero-paired tails from KLP-20 and KLP-11. KAP-1 adopts an elongated superhelical structure featuring a central target-binding groove and a C-terminal helical (CTH)-hook. The two distinct motor tails fold together in a complementary manner and are co-sequestered within the target-binding groove of KAP-1. The adjacent hetero-pairing trigger sequences (HTS segments) preceding the two tails are assembled into an intertwined heterodimer that specifically co-recognizes the CTH-hook of KAP-1. Mutations in the inter-subunit interfaces between KAP-1 and the two motor tails disrupt the heterotrimeric kinesin-2 complex and impair kinesin-2-mediated intraflagellar transport. Thus, KAP-1 and the two hetero-paired tails are mutually co-recognized, ensuring the proper assembly of heterotrimeric kinesin-2 for cargo transport.

Results

Biochemical assembly of the KLP-20/KLP-11/KAP-1 complex without motor domains

To investigate the mechanism underlying the assembly of heterotrimeric kinesin-2, we initiated this study with the biochemical assembly and characterization of the KLP-20/KLP-11/KAP-1 complex from *Caenorhabditis elegans*, in which KLP-20 and KLP-11 are the two motor proteins and KAP-1 is the accessory protein (Fig. 1a). Based on earlier electron microscopy (EM) studies of heterotrimeric kinesin-2[25,26], it was established that the accessory protein KAP primarily associates with the C-terminal tails of the two motor proteins rather than their N-terminal motor domains. Moreover, the overall conformation of the holoenzyme exhibited an extended architecture with intrinsic dynamic properties caused by the coiled-coil stalk. Since the primary focus of this work was to dissect the holoenzyme assembly mediated by KAP-1 and the motor tails of KLP-20 and KLP-11, we chose to remove the two motor domains and the N-terminal sections of coiled-coil stalks (including the neck coil and coiled-coil 1) (Fig. 1a). This modification was intended to minimize any unfavorable impact that these domains might have on our structural studies. In contrast, we retained the second and third coiled-coils (CC2-CC3) of the two motor proteins due to their potential interactions with the accessory protein[28]. Thus, the resulting heterotrimeric complex for structural characterization was composed of the CC2-CC3-Tail domains of KLP-20 and KLP-11 (referred to as K20-CC-Tail and K11-CC-Tail, respectively) along with full-length KAP-1 (Fig. 1a).

The initial attempts to mix the three proteins for assembling the heterotrimeric complex were unsuccessful, because each protein, especially KAP-1, was difficult to produce when expressed individually. Consequently, we opted to co-express them using the baculovirus expression system and obtained the K20-CC-Tail/K11-CC-Tail/KAP-1 complex. This complex was observed to co-elute as a single peak in the analytical gel-filtration analysis (Supplementary Fig. 1a). Based on the high quality of this co-purified complex, we proceeded with crystal screening. However, all attempts were unsuccessful, likely due to the presence of the coiled-coils (CC2-CC3), which were unfavorable for crystallization (Fig. 1a). To obtain structural information about the K20-CC-Tail/K11-CC-Tail/KAP-1 complex, we turned to cryo-electron microscopy (cryo-EM).

Cryo-EM analysis of the K20-CC-Tail/K11-CC-Tail/KAP-1 complex

We visualized the K20-CC-Tail/K11-CC-Tail/KAP-1 complex using cryo-EM and aimed to determine its structure through the single-particle method (Fig. 1b and Supplementary Fig. 1b). However, the presence of pronounced preferred orientations of the complex hindered our ability to obtain a high-resolution structure (Supplementary Fig. 1c). The cryo-EM map of the K20-CC-Tail/K11-CC-Tail/KAP-1 complex was reconstructed, and the 3D-FSC analysis revealed a global resolution of 4.9 Å with a sphericity value of 0.768, consistent with preferential orientations (Supplementary Fig. 1c–f and Supplementary Table 1). The reconstructed cryo-EM map revealed that the overall conformation of the complex is predominantly composed of α-helices, with the helices in the central core exhibiting a higher local resolution (Supplementary Fig. 1d–g). Based on primary sequence analysis and structural prediction, KAP-1, the primary component of the complex, was identified as an armadillo (ARM)-repeat-containing protein that adopts a superhelical structure. Consistently, most of the helices in the complex are organized into a superhelical arrangement with a right-handed twist (Fig. 1c), similar to other ARM-repeat-containing proteins.

Motor tails and adjacent hetero-pairing trigger sequences for association with KAP-1

Given that the resolution of the cryo-EM map of the K20-CC-Tail/K11-CC-Tail/KAP-1 complex was insufficient to construct an atomic model, we aligned the structural model of KAP-1 predicted by AlphaFold2 with the density map to analyze the complex assembly (Fig. 1d and Supplementary Fig. 2). The solenoid ARM-repeats with the characteristic triangular arrangement of helices were clearly identified, allowing the well-fitting of the central portion of KAP-1 into the density map of the complex (Fig. 1d). This structure-based alignment confirmed that the superhelical structure of the complex is constructed by KAP-1. In contrast, the N-terminal region of KAP-1 could not dock into and was missing from the density map (Supplementary Fig. 2). Based on the well-fitted ARM-repeats of KAP-1 in the density map, we observed additional unassigned elongated densities that bind to and span across the concave groove of the ARM-repeats (Fig. 1d), unlikely attributable to KAP-1. Given this spatial organization and the nature of the heterotrimeric complex, we tentatively assigned these extra densities as the motor tails of KLP-20 and KLP-11 (see below for details).

On the other hand, although the coiled-coil domains (CC2-CC3) of the two motor proteins were included in the complex, no long, extended rod-like densities were observed in the cryo-EM map, suggesting that the majority of CC2-CC3 is flexible and lacks a fixed orientation (Fig. 1d, e). Instead, additional rod-like densities contact and protrude from the C-terminal end of KAP-1, resembling an extended tail of the superhelical structure (Fig. 1b–d). These densities were most likely contributed by the extreme C-terminal end of CC3, specifically the adjacent coiled-coil preceding the motor tail, which has been previously identified as the HTS segment[10] (Fig. 1a). Thus, the cryo-EM map of the heterotrimeric complex demonstrated that the ARM-repeats of KAP-1 form a central scaffold that likely associates with the

https://doi.org/10.1038/s41467-025-62152-8

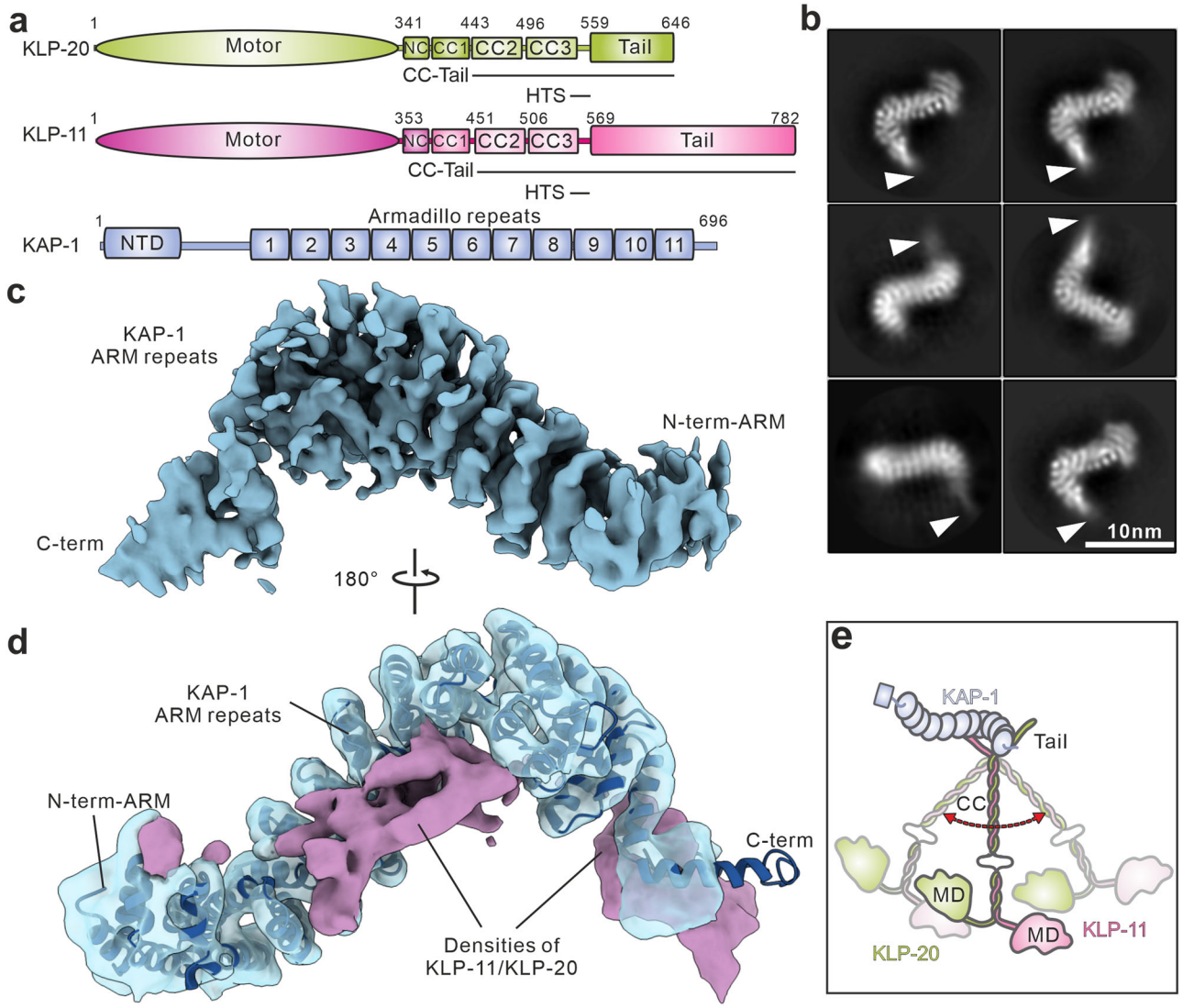

Fig. 1 | Cryo-EM characterization of the K20-CC-Tail/K11-CC-Tail/KAP-1 complex. a Domain organization of KLP-20, KLP-11 and KAP-1. Both KLP-20 and KLP-11 contain an N-terminal motor domain, a neck coil (NC), the coiled-coil stalks (CC1–CC3) followed by a C-terminal tail domain. HTS, hetero-pairing trigger sequence. KAP-1 contains 11 armadillo (ARM) repeats and a N-terminal domain (NTD) with unknown functions. The residues numbers for each domain are indicated above the domain organization. Protein constructs used for cryo-EM characterization are marked by lines under the domain organization. **b** Representative 2D-classification averages of cryo-EM datasets. The white arrow-heads indicate the orientation of the coiled-coil stalks. **c** Cryo-EM reconstruction of the K20-CC-Tail/K11-CC-Tail/KAP-1 heterotrimeric complex, showing distinctive ARM-repeat structural features. **d** Segmentation of the cryo-EM reconstruction of the K20-CC-Tail/K11-CC-Tail/KAP-1 complex. The EM density corresponding to KAP-1 is shown in dark cyan with the extra EM densities shown in pink. The AlphaFold2-predicted KAP-1 structural model is fitted into the cryo-EM density map. **e** Schematic model of the KLP-20/KLP-11/KAP-1 complex showing the intrinsic flexibilities of the N-terminal region of KAP-1 and the flexible CC2-CC3 orientation of the KLP-20/KLP-11 motor heterodimer.

motor tails of KLP-20 and KLP-11, as well as their adjacent HTS segments, to facilitate the complex assembly (see below for details).

Crystallization of the K20-HTS-Tail/K11-HTS-Tail/KAP-1ΔN complex

Since the high-resolution structure of the K20-CC-Tail/K11-CC-Tail/KAP-1 complex was unable to be obtained through cryo-EM, we decided to crystallize the structural core of this heterotrimeric complex. The cryo-EM analysis indicated that the structural core mainly comprises the ARM-repeats of KAP-1, the motor tails of KLP-20 and KLP-11, and their HTS segments (Fig. 1d). To facilitate crystallization, we truncated the N-terminal region of KAP-1 (designated KAP-1ΔN) and shortened CC2-CC3-Tail while retaining the HTS segments of KLP-20 and KLP-11 (referred to as K20-HTS-Tail and K11-HTS-Tail). This resulted in a mini-heterotrimeric complex possibly suitable for structural studies (Fig. 2a). The K20-HTS-Tail/K11-HTS-Tail/KAP-1ΔN complex was obtained through co-expression using a bacterial expression system and characterized by the size-exclusion chromatography coupled with multi-angle light-scattering (SEC-MALS) assay (Fig. 2b). As anticipated, the calculated molecular weight of the complex indicated a stoichiometry of 1:1:1 of the three proteins, confirming the formation of the complex (Fig. 2b). Based on the high quality of the protein sample, we proceeded with crystal screening of the complex. After extensive trials, we obtained crystals of the complex for structural determination.

Crystal structure of the K20-HTS-Tail/K11-HTS-Tail/KAP-1ΔN complex

The structure of the K20-HTS-Tail/K11-HTS-Tail/KAP-1ΔN complex was determined using the molecular replacement method, with the AlphaFold2-predicated structural model of the ARM-repeats of KAP-1 serving as the searching model. The final structure was refined to 3.5 Å (Fig. 2c and Supplementary Table 2). Consistent with the biochemical

https://doi.org/10.1038/s41467-025-62152-8

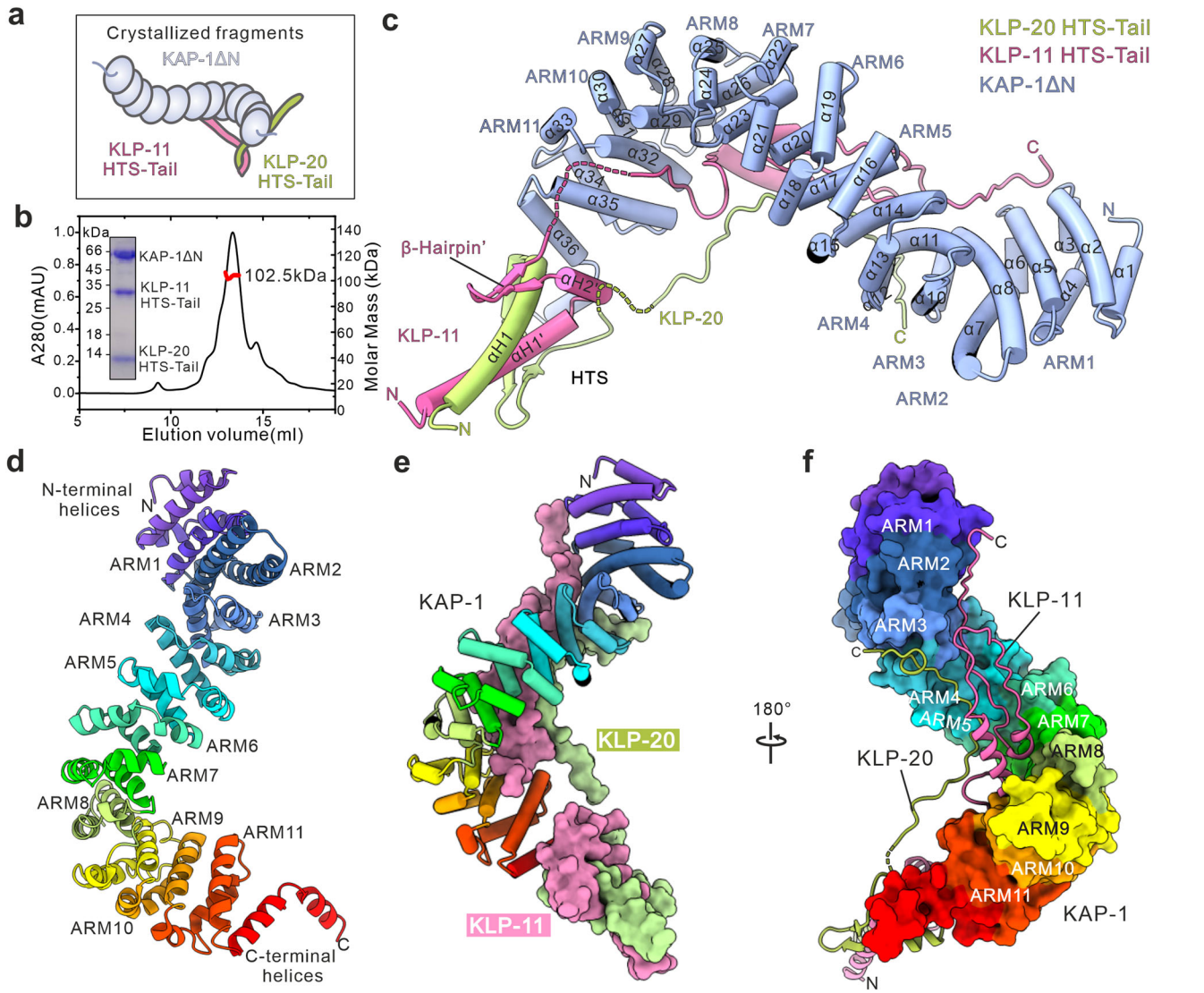

Fig. 2 | Crystal structure of the K20-HTS-Tail/K11-HTS-Tail/KAP-1ΔN complex. **a** Illustration of the protein constructs used for crystallization. KAP-1ΔN, K20-HTS-Tail and K11-HTS-Tail form a mini-heterotrimeric complex for structural studies. **b** Biochemical characterization of the K20-HTS-Tail/K11-HTS-Tail/KAP-1ΔN complex by SEC-MALS. The calculated molecular weight corresponds to a heterotrimeric state with a stoichiometry of 1:1:1 for each component. The inset shows the SDS-PAGE analysis of each component. The experiment is independently repeated three times ($n = 3$). Source data are provided as a Source Data file. **c** A ribbon diagram of the K20-HTS-Tail/K11-HTS-Tail/KAP-1ΔN complex structure. In this drawing, KLP-20, KLP-11 and KAP-1 are colored in green, pink and blue, respectively. **d** A rainbow-colored diagram of the KAP-1ΔN structure, with a gradient transitioning from blue at the N-terminus to red at the C-terminus. KAP-1ΔN is composed of N-terminal helices (NTH, α1 and α2), eleven helix-based ARM-repeats (ARM1 to ARM11, α3 to α35) and C-terminal helices (CTH, α36 and α37). **e**, **f** A combined surface and ribbon diagram of the K20-HTS-Tail/K11-HTS-Tail/KAP-1ΔN complex.

characterization in solution, only one molecule of each protein was found in the complex structure (Fig. 2b, c). In the complex structure, the electron density maps of most regions were of high quality to allow reliable model building (Supplementary Fig. 3a, b). However, the extreme C-terminal tails of KAP-1ΔN, K20-HTS-Tail, and K11-HTS-Tail, as well as the internal flexible loops in K20-HTS-Tail and K11-HTS-Tail (as indicated by dashed lines in Fig. 2c), could not be resolved due to poor electron density (Supplementary Fig. 3a). Thus, the resolved structure included KAP-1ΔN with residues 123–679, K20-HTS-Tail with residues 531–624, and K11-HTS-Tail with residues 537–721 (Fig. 2c).

In the heterotrimeric complex structure, KAP-1ΔN is composed of eleven helix-based ARM-repeats (ARM1 to ARM11, α3 to α35) that are arranged in an elongated superhelical conformation featuring a characteristic concave groove (Fig. 2d, e). Additionally, two N-terminal helices (NTH, α1 and α2) tightly pack against the first ARM-repeat, sealing the N-terminal end of KAP-1ΔN, while two C-terminal helices (CTH, α36 and α37) loosely contact with the last ARM-repeat, resembling a hook that extends from the C-terminal end of KAP-1ΔN (Fig. 2d). On the other hand, the two HTS segments from K20-HTS-Tail and K11-HTS-Tail form an intertwined heterodimer (rather than a canonical coiled-coil structure), which specifically captures the CTH-hook of KAP-1ΔN (Fig. 2e, f). This intertwined HTS heterodimer sequesters the CTH-hook of KAP-1ΔN and further extends the superhelical conformation of the complex (Fig. 2e, f). In contrast, the motor tails of K20-HTS-Tail and K11-HTS-Tail do not exhibit specific structural features but fold together to span across the elongated groove of KAP-1ΔN, and KAP-1ΔN resembles a twisted clamp that colligates the two motor tails and locks them into a fixed conformation (Fig. 2e, f). Thus, K20-HTS-Tail and K11-HTS-Tail form a unique heterodimer that is co-recognized and tightly interlocked with KAP-1ΔN, resulting in the assembly of an integrated heterotrimeric complex.

https://doi.org/10.1038/s41467-025-62152-8

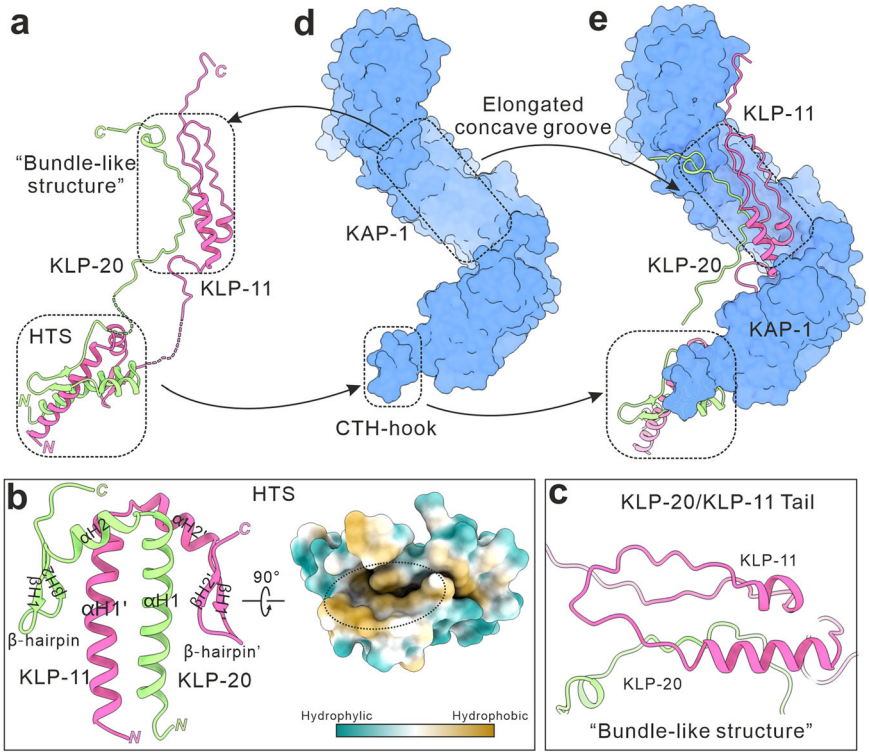

Fig. 3 | Co-recognition of K20-HTS-Tail and K11-HTS-Tail by KAP-1ΔN for assembling the heterotrimeric complex. a A ribbon diagram of the crystal structure of the K20-HTS-Tail/K11-HTS-Tail heterodimer showing an intertwined HTS heterodimer and a bundle-like structure formed by the two motor tails (indicated by dashed boxes). **b**, **c** A close-up view of the intertwined HTS heterodimer (**b**) and a bundle-like structure (**c**) of the K20-HTS-Tail/K11-HTS-Tail heterodimer. **d** Surface representation of the KAP-1ΔN structure showing the central concave groove in the middle and a C-terminal CTH-hook. **e** Co-recognition of K20-HTS-Tail and K11-HTS-Tail by KAP-1ΔN. The central groove of KAP-1ΔN co-recognizes the motor tails of KLP-20 and KLP-11, acting as a clamp to grasp the bundle-like structure. Meanwhile, the CTH-hook of KAP-1ΔN inserts into a pocket at the top of the HTS heterodimer, enabling mutual co-recognition to complete the assembly of the heterotrimeric complex.

We fitted this structure into the cryo-EM map of the K20-CC-Tail/K11-CC-Tail/KAP-1 complex to evaluate the previously unassigned densities (Supplementary Fig. 3c). As anticipated, all three proteins in the complex could be aligned with the density map, with the best fit provided by the ARM-repeats of KAP-1ΔN, rather than the HTS heterodimer (Supplementary Fig. 3c). The previously unassigned densities within the concave groove of KAP-1ΔN were indeed contributed by the motor tails of K20-HTS-Tail and K11-HTS-Tail, while the densities protruding from the ARM-repeats of KAP-1ΔN were associated with the HTS heterodimer (Supplementary Fig. 3c), confirming the above tentative assignment (Fig. 1d). Notably, the obvious tilting of the HTS heterodimer deviated from the cryo-EM map suggests its intrinsic flexibility, likely caused by random rotation of the central coiled-coil stalk within the heterotrimeric motor (Supplementary Fig. 3c and Fig. 1e). Therefore, the crystal structure of the K20-HTS-Tail/K11-HTS-Tail/KAP-1ΔN complex is consistent with the cryo-EM map of the K20-CC-Tail/K11-CC-Tail/KAP-1 complex. Additionally, these structural fitting data support the previous assumptions regarding the structural core of the heterotrimeric complex, as well as the intrinsic flexibilities of the N-terminal region of KAP-1 and the orientation of the CC2-CC3 domains (Fig. 1e).

Hetero-pairing between K20-HTS-Tail and K11-HTS-Tail

In the K20-HTS-Tail/K11-HTS-Tail/KAP-1ΔN complex, a prominent structural feature is the intertwined HTS heterodimer that mediates the hetero-pairing between K20-HTS-Tail and K11-HTS-Tail (Fig. 3a), consistent with recent studies of this segment[29]. The HTS segment of each motor protein exhibits a similar structural topology, consisting of two helices (αH1 and αH2) and two strands (βH1 and βH2) that form a β-hairpin structure (Fig. 3b). In the intertwined HTS heterodimer, the two αH1 helices from the motor proteins form a canonical coiled-coil dimer, while the αH2 helix and β-hairpin from one motor protein wrap around the αH1 helix from the other, thereby fastening the central coiled-coil dimer (Fig. 3b). Since the HTS segment is located at the extreme C-terminal end of CC3 (Fig. 1a), this HTS heterodimer not only initiates the hetero-pairing but also resembles a compact knob that ties up the C-terminal end of the coiled-coil stalk, reinforcing the motor dimer (Fig. 1e). Thus, consistent with previous studies, the HTS segment is a key site for the hetero-pairing of two distinct motor proteins, and the intertwined assembly mode may ensure their proper heterodimerization.

In the HTS heterodimer, the hetero-pairing interfaces between the αH1 coiled-coil dimer are primarily formed by hydrophobic residues from the two helices, while two hydrophilic residues (N550 in KLP-20 and K560 in KLP-11) are positioned centrally and may be unfavorable for coiled-coil formation (Supplementary Fig. 4a). On the other hand, the hydrophobic residues from the αH2 helix and β-hairpin further pack with the hydrophobic residues at the C-terminal end of the αH1 helix, creating a continuous wrap around the coiled-coil dimer (Supplementary Fig. 4b). Notably, two characteristic tryptophan residues (W572 and W579 in KLP-20; W582 and W589 in KLP-11) from the β-hairpin align tightly with a lysine and a leucine residue (K555 and L559 in KLP-11; K545 and L549 in KLP-20) from the αH1 helix, forming a W-W-K-L cluster that secures and locks the HTS heterodimer (Supplementary Fig. 4b). More importantly, most of the residues responsible for the assembly of the HTS heterodimer (especially those in the W-W-K-L cluster) are highly conserved among other kinesin-2 family proteins (Supplementary Fig. 4c). This suggests that the HTS heterodimer may represent a common structural feature for hetero-pairing or homo-paring

between motor proteins in the kinesin-2 family. Consistent with this assumption, structural models (predicated by AlphaFold3) of similar HTS segments from other kinesin-2 motors (such as KIF3A/KIF3B, KIF3A/KIF3C, KIF17 and OSM-3) indeed adopt a similar dimeric conformation (Supplementary Fig. 4d), This supports the notion that the HTS heterodimer or homodimer may serve as a common site for hetero-pairing or homo-paring, critical for regulating kinesin-2 dimerization. Furthermore, the HTS heterodimer features a deep hydrophobic pocket formed by both KLP-20 and KLP-11 at the top of this heterodimer (Fig. 3b), suggesting that this segment may recognize other potential partners, such as KAP-1, as demonstrated in the complex structure (Fig. 2c and see below for details).

In addition to the HTS segment, the flexible motor tails of KLP-20 and KLP-11 in the K20-HTS-Tail/K11-HTS-Tail/KAP-1ΔN complex exhibit a unique hetero-pairing pattern (Fig. 3a). Since the motor tail of KLP-20 is significantly shorter than that of KLP-11 (Fig. 1a), the motor tail of KLP-11 folds back and forth to specifically hetero-pair with the shorter tail of KLP-20, resulting in a bundle-like structure (Fig. 3c). Specifically, three residues (N606, Q607 and T608) from the motor tail of KLP-20 insert into a pocket formed by the folded tail of KLP-11, establishing a hydrogen-bonding network with the sidechains and backbones of residues (R668, N701 and F705) from the motor tail of KLP-11 (Supplementary Fig. 4e). Additionally, the sidechain of R668 from the motor tail of KLP-11 forms a reciprocal hydrogen-bonding interaction with the backbone of S603 from the motor tail of KLP-20, further stabilizing the hetero-pairing (Supplementary Fig. 4e). Notably, although the two motor tails contain several short helices in the complex structure, they do not form a stable helical-bundle conformation. Instead, the hetero-paired bundle-like structure is primarily assembled from the major linear portions of the tails (Fig. 3c), suggesting a potential instability in this linear bundle that may require additional regulators for stabilization. Consistently, the bundle-like structure formed by the flexible motor tails of KLP-20 and KLP-11 can be co-recognized by the accessory protein KAP-1, facilitating the assembly of the heterotrimeric holoenzyme (Fig. 2c and see below for details).

Unique co-recognition of K20-HTS-Tail and K11-HTS-Tail by KAP-1ΔN

In the K20-HTS-Tail/K11-HTS-Tail/KAP-1ΔN complex, KAP-1ΔN serves as the central scaffold, primarily constructed from the ARM-repeats that form an elongated superhelical conformation (Fig. 3d). The superhelical characteristics of KAP-1ΔN create an intrinsic elongated concave groove in the center, which is conducive to recognizing its binding partners (Fig. 3d). Upon the hetero-pairing of K20-HTS-Tail and K11-HTS-Tail, the central groove of KAP-1ΔN specifically co-recognizes the motor tails of KLP-20 and KLP-11, driving them to fold together and grasping the bundle-like structure formed by the motor tails (Fig. 3e). Given that the isolated bundle-like structure appears to be unstable (Fig. 3c), the clamping action of KAP-1ΔN would facilitate its specific assembly, and KAP-1ΔN likely acts as a platform to initiate and stabilize the hetero-pairing between the two flexible motor tails (Fig. 3e). On the other hand, in the absence of its hetero-pairing partner, the single motor tail is unlikely to be properly recognized by the central groove of KAP-1ΔN due to potential association defects (see Discussion below). Thus, the co-recognition of the K20-HTS-Tail and K11-HTS-Tail by KAP-1ΔN may ensure the specific hetero-pairing between the two motor tails and facilitates the proper assembly of the motor complex for cargo transport.

Since the formation of an elongated central groove is a characteristic structural feature of ARM-repeat-containing proteins, we next compared the structure of KAP-1ΔN with that of other known ARM-repeat-containing proteins, such as importin and catenin (Supplementary Fig. 5a). The superhelical conformation of KAP-1ΔN is similar to that of these proteins, which also possess a central target-binding groove (Supplementary Fig. 5a). However, unlike the shallow grooves found in importin and catenin, the central groove of KAP-1ΔN is much deeper and broader. Consequently, the target-binding grooves in importin and catenin can only recognize a linear sequence motif, whereas the central groove in KAP-1ΔN is capable of accommodating the bundle-like structure formed by two motor tails with more buried surface areas (Supplementary Fig. 5a). Thus, we assume that the intrinsic physical properties of the central groove in KAP-1ΔN may enable this ARM-repeat-containing protein to co-recognize the two motor tails rather than merely a linear sequence motif (see Discussion below). This co-recognition mechanism distinguishes KAP-1ΔN from the target-binding modes of other ARM-repeat-containing proteins (Supplementary Fig. 5a).

More intriguingly, compared to other ARM-repeat-containing proteins, KAP-1ΔN features a unique C-terminal CTH-hook that extends from its superhelical conformation (Supplementary Fig. 5a). This CTH-hook can be co-captured by the pre-assembled HTS heterodimer of KLP-20 and KLP-11, resembling a torch igniting the CTH-hook (Fig. 3d, e). In this distinctive recognition, the CTH-hook of KAP-1ΔN specifically inserts into a deep pocket formed at the top of the HTS heterodimer (Fig. 3b and see below interface analysis). Thus, in addition to the co-recognition of the two motor tails by the central groove of KAP-1ΔN, the HTS heterodimer is also capable of co-capturing the CTH-hook, thereby completing the assembly of the heterotrimeric complex (Fig. 3e). This mutual co-recognition between KAP-1 and the two motors ensures the proper assembly of heterotrimeric kinesin-2 for intraflagellar transport.

Inter-subunit interfaces between KAP-1ΔN and two motor tails

Based on the mutual co-recognition between KAP-1 and the two motor tails, the inter-subunit interfaces can be categorized into two sites: the ARM-mediated site (interface I) and the CTH-hook-mediated site (interface II) (Fig. 4a). The ARM-mediated interface I can be further divided into three sub-categories based on different ARM repeats from the N-terminus to the C-terminus (interface Ia to Ic) (Fig. 4b–d). Specifically, in interface Ia, hydrophobic residues (I269, L273 and V276) from KAP-1 ARM3 form interactions with the tyrosine-rich segment of KLP-20 (^{612}YYSYRADL^{619}), as well as residues I679 and L708 from KLP-11. Additionally, residue E314 from KAP-1 establish a hydrogen-bonding/electrostatic network with residues S614 and R616 from KLP-20. The bulky sidechain of K316 from KAP-1 aligns with Y612 from KLP-20, and Y613 from KLP-20 leans against R710 from KLP-11, thereby stabilizing this interface (Fig. 4b and Supplementary Figs. 6, 7). In interface Ib, residues F348 and F352 from KAP-1 ARM4, Y384 and L385 from ARM5, and A420 and L423 from ARM6 form hydrophobic contacts with M611 from KLP-20, as well as residues I690, V702, V703, F705 and L708 from KLP-11. Additionally, residues N424 and N349 from KAP-1 form a hydrogen-bonding network with N701 and the backbone of E709 from KLP-11, thereby tightly integrating the interaction interface (Fig. 4c and Supplementary Figs. 6, 7). In interface Ic, residues I559, Y600 and V636 from KAP-1 ARM9-11 form hydrophobic contacts with residues L646, V647 and P655 from KLP-11. Additionally, F602 from KLP-20 interacts with M656 and R661 from KLP-11. Moreover, residue D390 from KAP-1 forms an electrostatic network with residues R653 and E700 from KLP-11, thus locking the inter-subunit interface (Fig. 4d and Supplementary Figs. 6, 7). Notably, in contrast to the favorable interactions described above, some contacts in interface Ic appear to hinder the formation of the heterotrimeric complex. For instance, R654 from KLP-11 directly inserts into a positively charged pocket, leading to charge conflicts with K460 and R463 from KAP-1 (Supplementary Fig. 8a). Additionally, S657 from KLP-11 fits into a hydrophobic pocket where it is surrounded by several hydrophobic residues from KAP-1 (Supplementary Fig. 8b). These contacts suggest that they could destabilize the complex formation or serve as potential regulatory sites (see Discussion below).

https://doi.org/10.1038/s41467-025-62152-8

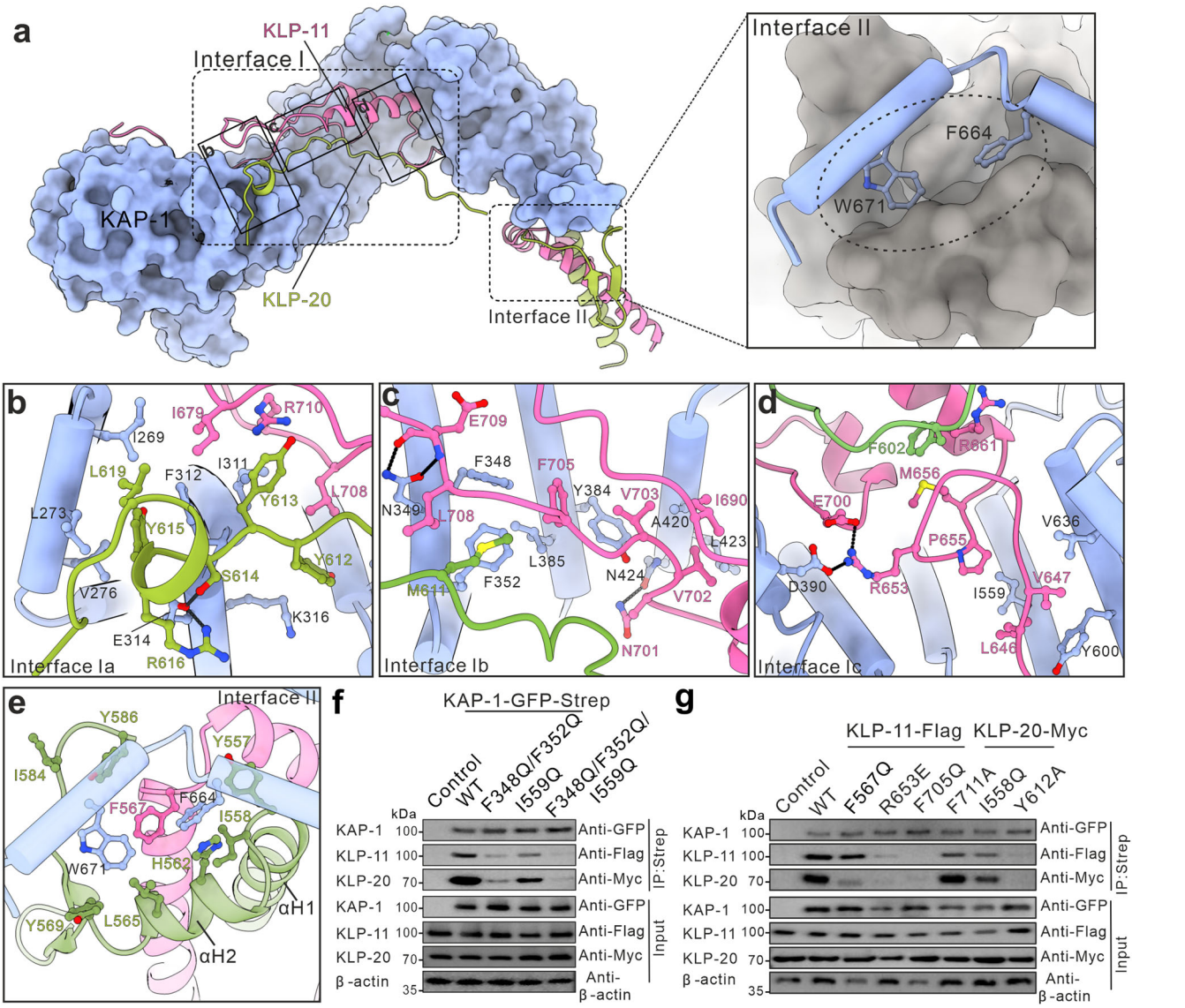

Fig. 4 | Inter-subunit interfaces between KAP-1ΔN and the two motor tails. a A combined surface and ribbon model showing the inter-domain interfaces that can be divided into two sites, the ARM-mediated site (interface I) and the CTH-hook-mediated site (interface II). **b**–**d** A combined ribbon and stick model showing the ARM-mediated interface I. Interface I is divided into three sub-categories (interface Ia (**b**), interface Ib (**c**) and interfaceIc (**d**) based on different ARM repeats from the N-terminus to the C-terminus). The sidechains of the key residues involved in the inter-domain interface packing are shown as sticks. **e** A combined ribbon and stick model showing the CTH-hook-mediated site (interface II). **f**, **g** Co-immunoprecipitation assay of KAP-1, KLP-20 and KLP-11 in Sf9 cells that are co-transfected with wild-type KAP-1-GFP-Strep, KLP-20-Myc and KLP-11-Flag and their various mutants. The modified pFastbac1 vector expressing the GFP-Strep tag is used as the negative control. Each experiment is independently repeated three times ($n = 3$). Source data are provided as a Source Data file.

In the CTH-hook-mediated interface II, the CTH-hook of KAP-1 contains two characteristic aromatic residues (F664 and W671) that closely associate with the HTS heterodimer of KLP-20 and KLP-11 (Fig. 4a). Specifically, residues F664 and W671 from the CTH-hook anchor into a deep hydrophobic pocket within the HTS heterodimer, forming hydrophobic interactions with the αH1/αH2-region of KLP-20 (Y557, I558, H562, L565, Y569, I584 and Y586), as well as F567 from KLP-11, thereby sealing this pocket (Fig. 4e and Supplementary Figs. 6, 7). Thus, the hydrophobic pocket within the HTS heterodimer is formed by residues from both motor proteins, indicating that this heterodimer must be preassembled to co-recognize the CTH-hook of KAP-1. Collectively, the inter-subunit interfaces between KAP-1 and the two motors are characterized by extensive hydrophobic, hydrogen-bonding and electrostatic interactions. Moreover, most of the residues involved in these inter-subunit interactions are highly conserved, and the interfaces are also largely contributed by all three proteins (Fig. 4b–e and Supplementary Figs. 6, 7), suggesting that this co-recognition may represent a common mechanism for the assembly of heterotrimeric kinesin-2.

Inter-subunit interfaces are essential for heterotrimeric kinesin-2 assembly

To evaluate the inter-subunit interfaces between KAP-1 and the two motors for the assembly of the heterotrimeric complex, we introduced a series of point mutations in KAP-1 (F348Q/F352Q and I559Q), KLP-20 (I558Q and Y612A) and KLP-11 (F567Q, R653E and F705Q) to disrupt the interaction interfaces among these proteins (Fig. 4b–e). Since each component of heterotrimeric kinesin-2 could not be effectively expressed and purified in isolation, we co-expressed the three full-length proteins in Sf9 cells and employed a co-immunoprecipitation assay to assess the complex formation (Fig. 4f, g). To ensure proper detection of each protein, KAP-1, KLP-20 and KLP-11 were fused with a

GFP-Strep, Myc and Flag tag, respectively, and were detected using the corresponding specific anti-tag antibodies. Interestingly, the double mutation F348Q/F352Q in KAP-1 largely impaired the complex formation, while the single mutation I559Q in KAP-1 caused only a slight dissociation of the heterotrimeric complex (Fig. 4f). The combination of three point-mutations (F348Q/F352Q/I559Q) at different sub-interfaces in KAP-1 resulted in the significant disassembly of the complex (Fig. 4f). This finding suggests that the extended concave groove of KAP-1 pays an essential role in the complex assembly, requiring multiple point mutations to disrupt its integrity.

On the other hand, the Y612A mutation in KLP-20 and the R653E and F705Q mutations in KLP-11 severely disrupted the complex formation, whereas the I558Q mutation in KLP-20 and the F567Q mutation in KLP-11 only slightly impaired the complex assembly (Fig. 4g). Since the latter two point-mutations are located in interface II (Fig. 4e), these results suggest that the CTH-hook-mediated interface II likely plays an auxiliary role, while the ARM-mediated interface I serves as the primary site for the complex assembly. Additionally, in interface I, the extreme C-terminal tail of KLP-11 further contacts with KAP-1 (Supplementary Fig. 8c), promoting us to introduce a point mutation (F711A) in this region. However, the F711A mutation had minimal impact on the complex assembly (Fig. 4g), indicating that this site may also only play a secondary role. Overall, these findings highlight the essential nature of the inter-subunit interfaces for the complex formation.

Evaluation of inter-subunit interfaces for kinesin-2-mediated intraflagellar transport

Based on the structure of the K20-HTS-Tail/K11-HTS-Tail/KAP-1ΔN complex, KAP-1 functions as a central scaffold that organizes the two motor tails to assemble heterotrimeric kinesin-2 (Fig. 4a). To assess the essential role of the inter-subunit interfaces in this heterotrimeric complex for kinesin-2-mediated intraflagellar transport (IFT), we introduced the point mutations in KAP-1 (F348Q/F352Q, I559Q and F348Q/F352Q/I559Q) to disrupt the inter-subunit interfaces (Fig. 4c, d). These KAP-1 mutants were expressed in the sensory cilia of *Caenorhabditis elegans* (Fig. 5a). In this model organism, slower heterotrimeric kinesin-2 (~0.5 μm/s) works in concert with faster homodimeric kinesin-2 (~1.3 μm/s) to construct the middle segments of cilia, resulting in an intermediate IFT velocity of ~0.7 μm/s. In the absence of heterotrimeric kinesin-2, homodimeric kinesin-2 becomes solely responsible for anterograde IFT, leading to an increased velocity in the middle segments to ~1.3 μm/s[30]. We crossed the *kap-1(ok676)* null allele with an IFT marker, *dyf-11::gfp*, which labels the entire cilium, and overexpressed wild-type *kap-1* and the *kap-1* mutants to determine if they could rescue the accelerated IFT phenotype observed in the *kap-1* null allele within the middle segments (Fig. 5b, c). As expected, wild-type *kap-1* fully rescued the accelerated IFT phenotype in the middle segments, resulting in an intermediate IFT velocity (0.76 ± 0.07 μm/s) (Fig. 5b, c). Both the *kap-1(I559Q)* and *kap-1(F348Q;F352Q)* mutants were able to reduce the IFT velocity in the middle segments to near wild-type levels, with the velocity of 0.77 ± 0.03 μm/s and 0.74 ± 0.03 μm/s, respectively (Fig. 5b, c). This suggests that neither of these two mutants is sufficient to eliminate the function of KAP-1. In contrast, the *kap-1(F348Q;F352Q;I559Q)* mutant, which carries multiple point mutations across different interfaces, failed to rescue the *kap-1* null allele. The IFT velocity remained elevated at 1.19 ± 0.04 μm/s, and the fluorescent signal of KAP-1(F348Q;F352Q;I559Q) did not enter the cilia, instead remaining localized to the dendrite endings (Fig. 5b, c). This observation indicates that the multiple point mutations in the inter-subunit interfaces lead to a loss of function in heterotrimeric kinesin-2, which aligns with that only a combination of multiple point mutations in KAP-1 results in severe disruption of the complex assembly (Fig. 4f). Thus, the inter-subunit interfaces in the heterotrimeric motor complex are crucial for kinesin-2-mediated intraflagellar transport.

Discussion

Among transport kinesins, heterotrimeric kinesin-2 is unique in its holoenzyme assembly, comprising two distinct motor proteins and an accessory protein KAP, which regulates intraflagellar transport and ciliogenesis[5,10]. The formation of heterotrimeric kinesin-2 necessitates the pre-assembly of the motor heterodimer[20], but the mechanism underlying the holoenzyme assembly remains unclear. In this study, we elucidate the structure of KAP-1 in complex with the two motor tails from kinesin-2 motors KLP-20 and KLP-11 (Fig. 2). This heterotrimeric complex structure reveals several features of kinesin-2 holoenzyme assembly. Firstly, the HTS segments from the two distinct motors specifically hetero-pair in a unique pattern, forming a torch-like intertwined heterodimer, which is distinct from the canonical coiled-coil dimer that forms the central stalk (Fig. 3). Secondly, while the two motor tails are flexible, they tend to fold together to create a hetero-paired bundle-like structure (Fig. 3). Thirdly, instead of binding to two separate sites, the two flexible motor tails can be co-recognized by KAP-1, which adopts a super-helical conformation with a broader groove to hold them together (Fig. 3). Fourthly, unlike other ARM-repeat-containing proteins, KAP-1 features an additional CTH-hook that can be co-captured by the HTS heterodimer, thereby securing the complex assembly (Fig. 3). Finally, the mutual co-recognition and interlocking between KAP-1 and the two motor tails, likely functioning as a form of “two-factor authentication”, can ensure the proper assembly of heterotrimeric kinesin-2 for cargo transport. These structural features will broaden our understanding of the assembly of heterotrimeric kinesin-2.

During the assembly of heterotrimeric kinesin-2, the specific hetero-pairing between the two distinct motors is intriguing due to their specialized internal segments required for the formation of the motor heterodimer[10]. Previous studies have demonstrated that the charge complementation between the two motors at the neck hinge and coiled-coil stalk is essential for dimerization[31,32], while the extreme C-terminal end of the coiled-coil stalk serves as the primary trigger site for hetero-pairing (i.e., the HTS segment)[24]. Here, we show that the specialized HTS segments of the two motors form an intertwined dimer, rather than a canonical coiled-coil, which ties up the extreme C-terminal end of the coiled-coil stalk (Figs. 2 and 3). Thus, this HTS heterodimer likely acts as a seed to initiate the hetero-pairing of the two motors and resembles a knob-like structure to seal the coiled-coil stalk (Fig. 1). Based on primary sequence analysis and AlphaFold3-based structural predictions, the HTS heterodimer appears to be a common feature of kinesin-2 motors in both homodimeric and heterodimeric states (Supplementary Fig. 4), underscoring the prominent role of this internal segment in motor dimerization. More intriguingly, in addition to the hetero-paring of the two motors, the HTS heterodimer features an additional target-binding site that recognizes the C-terminal CTH-hook of KAP-1 for the holoenzyme assembly (Fig. 3). This structural characteristic may help explain the necessity of a pre-assembled motor dimer for binding to KAP-1[20]. Further investigations are needed to determine whether the HTS segments of other kinesin-2 motors possess similar target-binding capacities.

In contrast to the intertwined HTS heterodimer, the two motor tails of heterotrimeric kinesin-2 appear too flexible to form a stable heterodimer and are unlikely to initiate motor dimerization (Fig. 3). Instead, they are sequestered and co-recognized by a target-binding groove within the superhelcial structure of KAP-1 (Fig. 3), which leads to the formation of a bundle-like structure. The simultaneous clamping of the two motor tails by KAP-1 facilitates their hetero-pairing, suggesting that KAP-1 may act as a motor dimerization regulator in addition to a cargo adaptor. Furthermore, due to the broader target-binding groove in KAP-1 compared to other ARM-repeat-containing proteins (Supplementary Fig. 5a), both motor tails may be necessary for a proper fit within this groove, and the absence of either tail would result in the dissociation of the heterotrimeric complex. To test this

https://doi.org/10.1038/s41467-025-62152-8

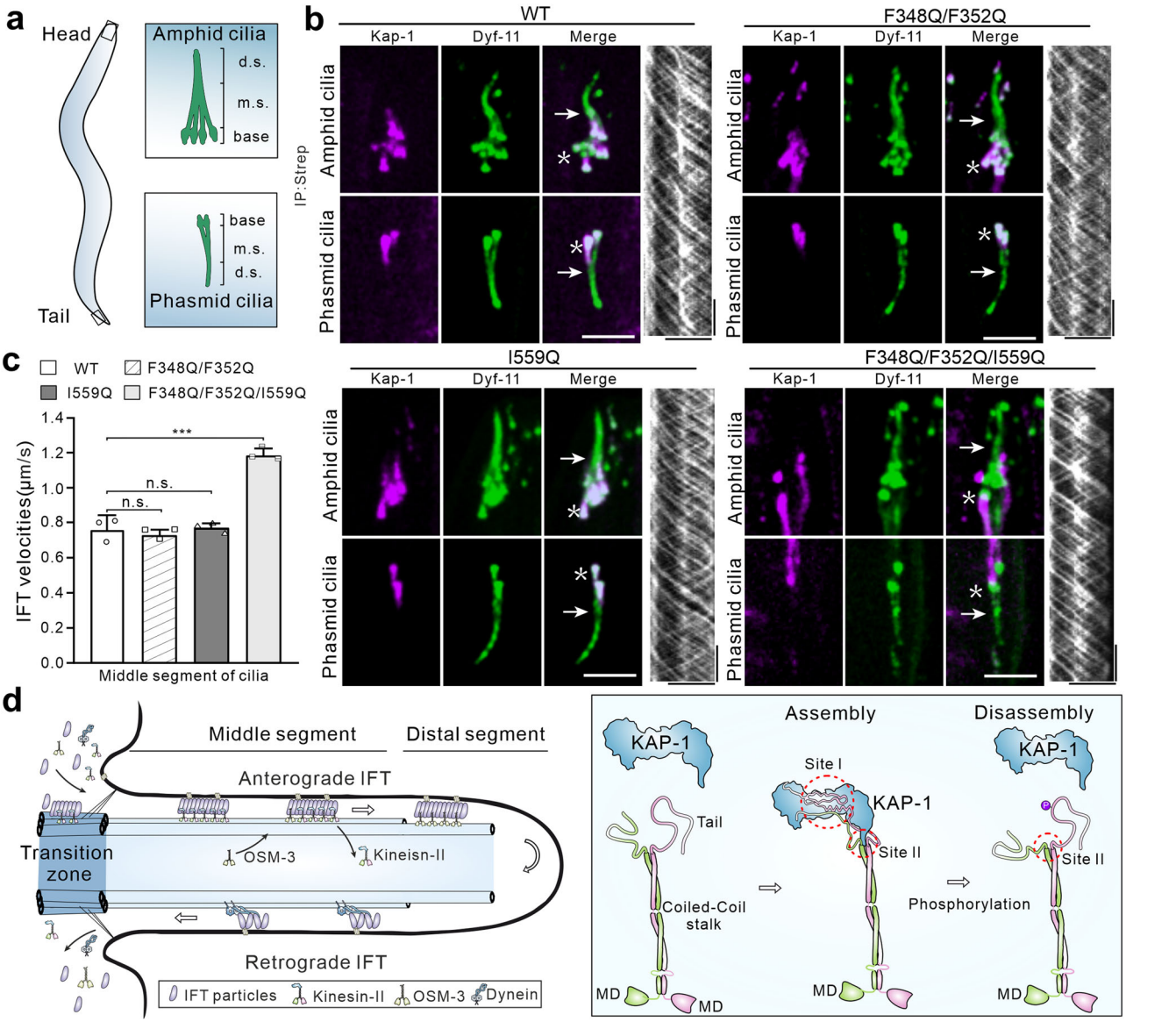

Fig. 5 | Evaluation of the inter-subunit interfaces for kinesin-2-mediated intraflagellar transport. a Diagram of sensory cilia (amphid cilia in the head and phasmid cilia in the lateral tail) on neurons of *C. elegans* (left). Right panel: the cartoon of section through amphid and phasmid cilia showing the longitudinal differentiation of sensory cilia into base, middle segments (m.s.) and distal segments (d.s.). **b** Rescue experiments of the accelerated IFT phenotype of the *kap-1* null allele by wild-type KAP-1 and its mutants. Fluorescence micrographs showing distribution of wild-type and mutant forms of Kap-1::Scarlet along long amphid (upper panels) and phasmid (lower panels) cilia in *kap-1(ok676)*; *dyf-11(cas1086)* worms. The middle-distal segment junction is indicated by an arrow. Asterisks indicate the ciliary base. Scale bar: 5 μm. Kymographs of intraflagellar transport along the middle segments of cilia are displayed at the far right of each panel. For the kymographs, the horizontal bars represent 5 μm, and the vertical bars represent 5 s. **c** Quantification of the IFT velocity in the middle segments of cilia. Each experiment is independently repeated three times ($n = 3$), with the data collected from at least 21 animals ($N \geq 21$) in each data set, and the average result is used to represent each experiment. Each bar represents the mean ± SD. n.s. no significant differences, $^{***}p < 0.001$, unpaired, two-tailed Student's *t* test. Exact *p*-values are listed in the Source Data file. Source data are provided as a Source Data file. **d** A schematic model illustrates the assembly of heterotrimeric kinesin-2 for intraflagellar transport. Before association with KAP-1, the motor tails of KLP-11 and KLP-20 remain flexible, while their HTS segments form an intertwined heterodimer to trigger the motor dimerization. This pre-assembled HTS heterodimer specifically captures the C-terminal CTH-hook of KAP-1 to initiate the complex assembly. During this process, the flexible motor tails are co-recognized by KAP-1 and fold together into the central groove of KAP-1, forming the heterotrimeric holoenzyme. Upon the potential phosphorylation of the motor tails, heterotrimeric kinesin-2 could be disassembled to release IFT cargoes and undergo a cycle of assembly and disassembly for intraflagellar transport.

hypothesis, we evaluated the binding between the single motor tail and KAP-1. Consistent with previous studies[20], neither KLP-20 nor KLP-11 alone was able to associate with KAP-1 (Supplementary Fig. 5b). Moreover, the point mutations in the central groove of KAP-1 could also disrupt the interactions with KLP-20 and KLP-11 (Fig. 4f), suggesting that both the wider shape and internal surface of this target-binding groove are likely critical for recognizing the two motor tails. Thus, the co-anchoring of the two motor tails into the central groove of KAP-1 necessitates the pre-assembly of the two motors into a heterodimer (Fig. 3), reinforcing the prerequisite of a heterodimeric motor for association with KAP-1[20]. Additionally, beyond the target-binding groove for specific co-recognition of the two motor tails, KAP-1 features an extra CTH-hook, which facilitates reciprocal association with the HTS heterodimer (Fig. 3). This CTH-hook is absent in other ARM-repeat-containing proteins (Supplementary Fig. 5a). Thus, KAP-1 is a unique member of ARM-repeat-containing proteins, possessing specific features for co-recognizing the two motor tails and regulating the motor dimerization.

Based on the structural features of KAP-1 and the two motor tails, they are mutually co-recognized within the heterotrimeric motor complex, with all three proteins contributing to the inter-subunit interfaces (Fig. 4). As KAP-1 serves as the central scaffold in the complex assembly, the inter-subunit interfaces are categorized into the ARM-mediated interface I and CTH-hook-mediated interface II (Fig. 4). The ARM-mediated interface I comprises the extensive inter-subunit interactions between KAP-1 and the two motor tails, likely making it the primary site for KAP-1 to assemble the heterotrimeric complex (Fig. 4). Biochemical mutational studies demonstrated that a single point mutation in interface I of KAP-1 only slightly impaired the complex formation. In contrast, only the combination of multiple point mutations across different sub-interfaces led to severe dissociation of the complex (Fig. 4), indicating that the target-binding groove of KAP-1 requires multi-site mutations to disrupt the association effectively. Consistently, functional evaluations of the inter-subunit interfaces revealed that the point mutations in one sub-interface of KAP-1 retained the activity of kinesin-2, likely due to residual association. Only the combination of multi-site mutations in KAP-1 resulted in significant impairment of kinesin-2-mediated intraflagellar transport (Fig. 5).

In comparison to the ARM-mediated interface I, the CTH-hook-mediated interface II exhibits fewer inter-subunit interactions between KAP-1 and the two motor tails (Fig. 4). Consistently, while the point mutations in the interface I of KLP-20 and KLP-11 caused severe impairments in the complex assembly, the point mutations in the interface II only resulted in mild decreases (Fig. 4). This supports the predominant role of the interface I in the motor complex assembly. Thus, the ARM-mediated interface I serves as the primary site for the assembly of heterotrimeric kinesin-2, while the CTH-hook-mediated interface II likely acts as an auxiliary site to aid this complex formation (Fig. 3). However, since the HTS heterodimer is pre-assembled for association with the CTH-hook, the CTH-hook-mediated interface II may also function as an initiation site that triggers the complex assembly, subsequently leading to the major association of the two motor tails with the central groove of KAP-1 (Fig. 3). Meanwhile, the interaction with KAP-1 further facilitates and stabilizes the dimer formation, suggesting that the motor dimerization and association with KAP-1 may be a synergetic process. This multi-site-mediated co-recognition between KAP-1 and the two motor tails may provide some advantages for regulating the intricate process of intraflagellar transport.

During kinesin-2-mediated intraflagellar transport in the sensory cilia of *Caenorhabditis elegans*, heterotrimeric kinesin-2 (Kinesin-II) tends to be disassembled at the end of the middle segment to hand over IFT cargos to homodimeric kinesin-2 (OSM-3) for transport to the tip of the distal segment (Fig. 5d)[16,30]. Consequently, heterotrimeric kinesin-2 undergoes a dynamic cycle of assembly and disassembly during intraflagellar transport. Interestingly, within the inter-subunit interfaces of the heterotrimeric complex structure, there are some contacts that disfavor the complex formation (Supplementary Fig. 8a, b). Potential charge conflicts in the interface Ic between the motor tail of KLP-11 and KAP-1 may destabilize the complex and contribute to the dynamic nature of the complex formation (Supplementary Fig. 8a). Accompanying this evident charge repulsion, a highly conserved serine residue in the motor tail of KLP-11 is positioned in the middle of the hydrophobic pocket in the interface Ic of KAP-1 (Supplementary Fig. 8b). We propose that the introduction of negative charges in this interface through the phosphorylation of this serine residue could impair the interaction interface and promote the complex dissociation. Previous studies demonstrated that KIF3B, a mammalian homolog of KLP-11, contains multiple potential phosphorylation sites including a serine residue that corresponds to this serine residue in KLP-11[33,34], likely supporting the assumption of phosphorylation-mediated regulation. Thus, the potential post-translational modification of this serine residue may represent an intriguing mechanism for regulating the dynamic disassembly of the motor complex in the middle segment (Fig. 5d), which warrants further validations and investigations.

Heterotrimeric kinesin-2 adopts an overall asymmetric architecture due to its unique holoenzyme assembly with three distinct proteins (Fig. 1e). More intriguingly, heterotrimeric kinesin-2 also exhibits asymmetric motility due to the distinct chemo-mechanical properties of its two motor domains (with different stepping kinetics)[18–20]. In this study, the structure of the heterotrimeric complex reveals that the two flexible motor tails of KLP-20 and KLP-11 can be co-recognized by KAP-1 (Fig. 2), which would fasten the motor tails and secure the holoenzyme in an asymmetric conformation. Although KAP-1 is far away from the motor domains and unlikely to directly affect the motor's kinetic properties (Fig. 1e), the KAP-1-mediated stabilization of the asymmetric architecture of the kinesin-2 holoenzyme may also somehow contribute to its asymmetric motility. On the other hand, during the KAP-1-mediated holoenzyme assembly, the initial contacts would happen between the pre-formed HTS dimer and the CTH-hook of KAP-1 (Fig. 5d). Upon the correct recognition between the HTS dimer and the CTH-hook, the two motor tails likely begin to fold together into the central groove of KAP-1 (Fig. 5d). Thus, in this "two-factor authentication" system, the binding between the HTS dimer and the CTH-hook works as the initial recognition step, while the co-folding of the two motor tails into the central groove of KAP-1 probably acts as the confirmation step for the holoenzyme assembly.

Finally, based on the structure of the heterotrimeric complex and the available data, we propose a working model for the assembly of heterotrimeric kinesin-2 for intraflagellar transport (Fig. 5d). In this model, the two motor tails of KLP-11 and KLP-20 remain flexible prior to their association with KAP-1, while the HTS segments of the two motors form an intertwined heterodimer that triggers the motor dimerization (Fig. 5d). Simultaneously, this pre-assembled HTS heterodimer co-captures the C-terminal CTH-hook of KAP-1, initiating the complex assembly. As this assembly progresses, the two flexible motor tails are further co-recognized by the ARM-repeats of KAP-1, allowing them to fold together into the central groove of KAP-1 to form the holoenzyme (Fig. 5d). This mutual co-recognition mechanism, akin to a "two-factor authentication" system, ensures the proper assembly of heterotrimeric kinesin-2 for cargo transport (Fig. 5d). In this process, KAP-1 may function as an adaptor for associating with cargoes as well as a regulator to stabilize the heterodimerization of kinesin-2. Upon the potential phosphorylation of the motor tails, heterotrimeric kinesin-2 could be disassembled, releasing IFT cargoes and allowing for a cycle of assembly and disassembly (Fig. 5d). This working model may serve as a starting point for further investigations into kinesin-2-mediated intraflagellar transport and ciliogenesis.

Methods

Protein expression and purification

DNA sequences encoding full length *Caenorhabditis elegans* KAP-1 were each cloned into a modified pFastBac1 (Gibco, 10359016) vector which contains a C-terminal GFP-His_6-Strep tandem tag. DNA sequences encoding the KLP-20-CC-Tail and KLP-11-CC-Tail were cloned into the multiple cloning site I (MCSI) and MCSII sites of the pFastBac-Dual vector (Gibco, 10712024), respectively. Primers used in this study were listed in Supplementary Table 3. The KLP-20-CC-Tail/KLP-11-CC-Tail/KAP-1 complex were expressed in insect sf9 cells (Gibco, 17-5318-03) using the Bac-to-Bac baculovirus expression system (Gibco, 10359016). Briefly, the plasmids were transformed into *Escherichia coli* DH10Bac cells (Gibco, 10359016) to acquire the bacmids. The P1 baculoviruses were obtained by transfecting the bacmids into sf9 cells using the Cellfectin II reagent (Gibco, 10362100), and the P2 baculoviruses were collected after 72 h of amplification from the P1 baculoviruses. For the large-scale production of the complex including three proteins, sf9 cells were cultured to a density of 2×10^6 cells/ml at 28 °C, and then coinfected with the with two baculoviruses. After the 72-h cultivation,

the cells were harvested and suspended in the buffer containing 50 mM Tris-HCl, pH 8.0, 500 mM NaCl, 5 mM imidazole. The proteins were purified by Ni^{2+}-Sepharose 6 Fast Flow (GE healthcare, 17-5318-03) affinity chromatography. The extra affinity purification was applied using the Strep-Tactin Sepharose resin (IBA Lifesciences, 2-1201-010) with the buffer containing 50 mM Tris-HCl, pH 8.0, 100 mM NaCl, 1 mM EDTA. After cleavage of the GFP-His_6-Strep tag, the proteins were further purified by size-exclusion chromatography (Superdex-200 10/300, Cytiva, 28990944) with the buffer containing 50 mM Tris-HCl, pH 8.0, 100 mM NaCl, 1 mM EDTA, 1 mM DTT.

DNA sequences encoding the *Caenorhabditis elegans* KAP-1ΔN were cloned into a pGEX-6p-1 vector (Shanghai Acmec Biochemical, AC13303) and those encoding the KLP-20-HTS-Tail and KLP-11-HTS-Tail were cloned into the MCSI and MCSII sites of a pCDFDuet-1 vector (Sigama, 71340-M), respectively. The pGEX-6p-1-KAP-1ΔN and pCDFDuet-1-KLP-20-HTS-Tail-KLP-11-HTS-Tail were cotransferred into *Escherichia coli* BL21 (DE3) cells for co-expression. Recombinant proteins were expressed at 16 °C. After the 18 h cultivation, the cells were harvested and suspended in the phosphate buffered saline. The proteins were purified using glutathione S-transferase (GST) resin affinity chromatography (GE healthcare, 17075601). After cleavage of the GST-tag, the resulting proteins were further purified by size-exclusion chromatography with the buffer containing 50 mM Tris-HCl, pH 8.0, 200 mM NaCl, 1 mM EDTA, 1 mM DTT.

Size exclusion chromatography coupled with multi-angle light scattering (SEC-MALS)

Protein samples (~1 mg/ml in 50 mM Tris-HCl, pH 8.0, 200 mM NaCl, 1 mM EDTA and 1 mM DTT) were analyzed with static light scattering by injection of them into an Agilent FPLC system with a Superdex-200 Increase 10/300 GL column (Cytiva, 28990944). The chromatography system was coupled with an 18-angle light-scattering detector (DAWN HELEOS II, Wyatt Technology) and a differential refractive index detector (Optilab rEx, Wyatt Technology). Masses (molecular weights) were calculated with ASTRA (Wyatt Technology). Bovine serum albumin (Sigma, 9048-46-8) was used as the calibration standard.

Cryo-EM sample preparation and data acquisition

Cryo-EM grids were prepared in the following manner using a Vitrobot Mark IV (FEI). R1/1 300-mesh grids (Zhongjingkeyi Technology, GIG-1010) were glow-discharged under O_2-Ar_2 for 1 min using a Gatan Plasma System. 3 µl protein samples (~0.1 mg/ml in 50 mM Tris-HCl, pH 8.0, 150 mM NaCl, 1 mM EDTA and 1 mM DTT) were applied to the glow-discharged grids for 10 s, followed by blotting for 7 s in the condition of 16 °C, 100% humidity. The grids were then plunge-frozen in liquid ethane using a Vitrobot Mark IV (Thermo Fisher Scientific). Data were collected using a Talos Arctica 200 kV machine (Thermo Fisher Scientific) equipped with a K2 Summit camera (Gatan) in the super-resolution mode at a nominal magnification of 130,000 and a pixel size of 1.0 Å, with a defocus range of −1.0 to −1.5 µm. Automated data acquisition was conducted using a modified SerialEM script to perform beam-image shift data collection[35]. The exposure time was 5.2 s, with a total exposure dose of 60 $e^-/Å^2$ over 32 frames.

Cryo-EM data analysis

Data processing steps were carried out using cryoSPARC[36]. The raw movie stacks underwent motion correction using Patch Motion, followed by contrast transfer function (CTF) estimation using Patch CTF. Particles were picked using Manual Picker, followed by Template Picker. A total of 2,134,786 particles were picked and extracted with a box size of 196 pixels and a binning factor of 2. Three rounds of 2D classification were then performed, resulting in the generation of 241,270 particles. The 3D ab initio reconstruction was conducted, and three classes were generated after two rounds of heterogenous refinement, with one class exhibiting relatively well-resolved structural features being chosen. The final map obtained through homogeneous refinement in CryoSPARC yielded a nominal resolution of 4.4 Å based on the gold-standard Fourier shell correlation (GSFSC) criterion (Supplementary Fig. 1d). However, due to the presence of preferred particle orientations, we reevaluated the resolution using the 3D-FSC analysis[37]. The resulting 3D-FSC profile showed a global resolution of 4.9 Å with a sphericity value of 0.768 (Supplementary Fig. 1f), indicating the moderate anisotropy of the cryo-EM map. Although the global FSC curve drops at around 4.9 Å with the 0.143 threshold, the wide spread of the green dashed line (corresponding to ±1 standard deviation) and the uneven distribution in the directional FSC histogram suggest the considerable directional variability in resolution (Supplementary Fig. 1f). The cryo-EM data processing workflow was summarized in Supplementary Fig. 1. The cryo-EM data collection and processing statistics were summarized in Supplementary Table 1. The structural model of KAP-1 was fitted into the corresponding cryo-EM density map by UCSF ChimeraX[38].

Crystallization, data collection and structural determination

Crystals of the KLP-20-HTS-Tail/KLP-11-HTS-Tail/KAP-1ΔN complex (12 mg/ml) were grown in 0.1 M HEPES, pH 7.8, 11% (w/v) PEG3350. All the crystals were obtained by using the sitting-drop vapor-diffusion method at 16 °C. Before being flash-frozen in liquid nitrogen, crystals were soaked in the mother liquor supplemented with 10% (w/v) di-ethylene glycerol for cryoprotection. Diffraction data were collected at the beamline BL02U1 at the Shanghai Synchrotron Radiation Facility (SSRF) with a wavelength of 0.979 Å at 100K[39], and were processed and scaled using HKL2000[40]. The structure of the complex was determined by the molecular replacement method with the predicted structure of KAP-1 from AlphaFold Protein Structure Database[41]. The AlphaFold2-predicted structural model was preprocessed by removing hydrogen atoms and the N-terminal residues before molecular replacement with Phaser[42]. The iterative model building was subsequently performed using COOT[43] and PHENIX[44] to gradually complete the structural model, which was continuously refined and improved through multiple cycles. In the early rounds of refinement, we focused primarily on maintaining the continuity of the main-chains, without assigning the side-chains. As the refinement progressed, the model improved, leading to the more accurate phase information and increasingly clearer electron density maps with the side-chains becoming resolved for most of the residues. Refinement of the molecular replacement solution gave rise to unambiguous extra densities attributing to KLP-20 and KLP-11. The AlphaFold2 model of KAP-1 was also used as a reference to assist in model building, particularly for those poorly resolved regions. The residues of KLP-20 and KLP-11 were then manually modeled into these electron densities using COOT. Although the K20-HTS-Tail (residues 527–646) and K11-HTS-Tail (residues 537–782) constructs were used for crystallization, the resolved regions of the two fragments are shorter and only include 87 and 142 residues, respectively, corresponding to the ordered regions of the HTS segment and large part of the motor tail. The structure was further refined with PHENIX. The structure figures were prepared with the program UCSF ChimeraX. The statistics for data collection and structural refinement were summarized in Supplementary Table 2.

Co-immunoprecipitation

DNA sequences encoding full length *Caenorhabditis elegans* KAP-1 and various mutants were cloned into a modified pFastBac1 vector which contains a C-terminal GFP-His_6-Strep tandem tag. DNA sequences encoding the full length and various mutants of Myc-tagged KLP-20 and Flag-tagged KLP-11 were cloned into the MCSI and MCSII sites of the pFastBac-Dual vector, respectively. To assess the binding of KAP-1 to the individual motor tail of KLP-20 or KLP-11, two additional pFastBac-Dual constructs were generated. In one construct, Myc-tagged KLP-20 was cloned into the MCSI site, leaving the MCSII site empty; in the other construct, Flag-tagged KLP-11 was inserted into the

MCSII site, leaving the MCSI site empty. Baculoviruses were produced individually for each plasmid following the procedures described above. Sf9 cells were coinfected with two baculoviruses. After a 60-h incubation, cells were harvested and lysed with RIPA lysis buffer (Beyotime, P0013C) supplemented with 1×Protease Inhibitors Cocktail (Lablead, P3441858), 250 U/ml BeyoZonase (Beyotime, D7121-100KU), 1 mM PMSF, 10 mM DTT. The cell lysates were cleared by centrifugation at 4 °C for 30 min. The supernatants were mixed with 10 µl anti-Strep beads (IBA Lifesciences, 2-1201-010) and incubated for 4 h at 4 °C. Subsequently, the beads were washed five times with the wash buffer (50 mM Tris-HCl, pH 8.0, 100 mM NaCl, 2 mM $MgCl_2$, 1 mM EGTA, 1 × Protease Inhibitors Cocktail, 1 mM PMSF, 10 mM DTT). For immunoblotting, HRP-conjugated mouse antibodies against GFP-tag (Beyotime, AF2885), Flag-tag (Beyotime, AF2852) and Myc-tag (Beyotime, AF2864) and HRP-conjugated rabbit antibodies against β-actin (Beyotime, AF5006) were employed. Chemiluminescent signals were imaged using Mini-Chemiluminescent Imager (MiniChemi 610 Plus, Beijing Sage Creation Science Co).

Genetics and microinjection

kap-1(ok676); dyf-11(cas1086) worm was generated by crossing *kap-1(ok676)* with *dyf-11::gfp(cas1086)*, and the genotype was confirmed by PCR and live imaging. DNA sequences encoding full length *Caenorhabditis elegans* KAP-1 and various mutants were cloned into a modified pOG44 vector (ThermoFisher, V600520) which contains a C-terminal mScarlet tag. Transgenic animals expressing wild type or corresponding mutant kap-1 were generated by co-inject the constructs with *rol-6(su1006)* into the germ line of young adult (YA) hermaphrodites of *kap-1(ok676); dyf-11(cas1086)* worms.

Live imaging

Fluorescence live imaging was performed following established procedures[45]. YA worms were anesthetized with levamisole and fixed on a 3% agarose pad. Then imaging was performed on an Axio Observer Z1 microscope (Carl Zeiss) equipped with a 100×, 1.49 NA objective, an electron-multiplying (EM) charge-coupled device (CCD) camera (Andor iXon+ DU-897D), and the 488/561 nm lines of a Sapphire CW CDRH USB Laser System attached to a spinning disk confocal scan head (Yokogawa CSU-X1 Spinning Disk Unit). Images were acquired by µManager (https://www.micro-manager.org) at an exposure time of 200 ms and analyzed with the software ImageJ (NIH). For IFT velocity measurements, IFT particles were randomly selected in amphid and phasmid cilia and measured by using kymographs.

Statistics and reproducibility

All blot experiments were independently repeated at least three times with similar results. Sample sizes (n) were indicated in the figure legends and represented independent biological replicates. For IFT velocity measurement, no statistical method was used to predetermine the sample size. The number of cilia analyzed was indicated in the figure legends, and the experiments were repeated independently three times with similar results. No data were excluded from the analyses. Statistical analyses were performed using two-tailed unpaired Student's t test. Data were presented as mean ± SD. Statistical analyses were conducted using Microsoft Excel (Microsoft, version 2021). A p-value < 0.001 was considered statistically significant.

Reporting summary

Further information on research design is available in the Nature Portfolio Reporting Summary linked to this article.

Data availability

The atomic coordinate of the KLP-20-HTS-Tail/KLP-11-HTS-Tail/KAP-1ΔN complex has been deposited in the Protein Data Bank with the accession code 9IKB. The three-dimensional cryo-EM density map of the KLP-20-CC-Tail/KLP-11-CC-Tail/KAP-1 complex has been deposited in the Electron Microscopy Data Bank under the accession code EMD-64192. The atomic coordinates used for structural comparison were downloaded from the Protein Data Bank with the accession codes 5SVZ, 1M1E, and 3L6X. Source data are provided with this paper.

References

1. Vale, R. D. The molecular motor toolbox for intracellular transport. *Cell* **112**, 467–480 (2003).
2. Soldati, T. & Schliwa, M. Powering membrane traffic in endocytosis and recycling. *Nat. Rev. Mol. Cell Biol.* **7**, 897–908 (2006).
3. Cason, S. E. & Holzbaur, E. L. F. Selective motor activation in organelle transport along axons. *Nat. Rev. Mol. Cell Biol.* **23**, 699–714 (2022).
4. Hirokawa, N., Noda, Y., Tanaka, Y. & Niwa, S. Kinesin superfamily motor proteins and intracellular transport. *Nat. Rev. Mol. Cell Biol.* **10**, 682–696 (2009).
5. Verhey, K. J., Kaul, N. & Soppina, V. Kinesin assembly and movement in cells. *Annu. Rev. Biophys.* **40**, 267–288 (2011).
6. Yildiz, A. Mechanism and regulation of kinesin motors. *Nat. Rev. Mol. Cell Biol.* **26**, 86–103 (2025).
7. Woehlke, G. & Schliwa, M. Walking on two heads: the many talents of kinesin. *Nat. Rev. Mol. Cell Biol.* **1**, 50–58 (2000).
8. Gennerich, A. & Vale, R. D. Walking the walk: how kinesin and dynein coordinate their steps. *Curr. Opin. Cell Biol.* **21**, 59–67 (2009).
9. Vale, R. D. & Fletterick, R. J. The design plan of kinesin motors. *Annu. Rev. cell Dev. Biol.* **13**, 745–777 (1997).
10. Scholey, J. M. Kinesin-2: a family of heterotrimeric and homodimeric motors with diverse intracellular transport functions. *Annu. Rev. Cell Dev. Biol.* **29**, 443–469 (2013).
11. Verhey, K. J. & Hammond, J. W. Traffic control: regulation of kinesin motors. *Nat. Rev. Mol. Cell Biol.* **10**, 765–777 (2009).
12. Gilbert, S. P., Guzik-Lendrum, S. & Rayment, I. Kinesin-2 motors: Kinetics and biophysics. *J. Biol. Chem.* **293**, 4510–4518 (2018).
13. Cole, D. G. et al. Novel heterotrimeric kinesin-related protein purified from sea urchin eggs. *Nature* **366**, 268–270 (1993).
14. Zhao, C., Omori, Y., Brodowska, K., Kovach, P. & Malicki, J. Kinesin-2 family in vertebrate ciliogenesis. *Proc. Natl Acad. Sci. USA* **109**, 2388–2393 (2012).
15. Engelke, M. F. et al. Acute inhibition of heterotrimeric kinesin-2 function reveals mechanisms of intraflagellar transport in mammalian cilia. *Curr. Biol.* **29**, 1137–1148.e1134 (2019).
16. Prevo, B., Mangeol, P., Oswald, F., Scholey, J. M. & Peterman, E. J. Functional differentiation of cooperating kinesin-2 motors orchestrates cargo import and transport in C. elegans cilia. *Nat. Cell Biol.* **17**, 1536–1545 (2015).
17. Zhang, Z., Danne, N., Meddens, B., Heller, I. & Peterman, E. J. G. Direct imaging of intraflagellar-transport turnarounds reveals that motors detach, diffuse, and reattach to opposite-direction trains. *Proc. Natl Acad. Sci. USA.* **118**, https://doi.org/10.1073/pnas.2115089118 (2021).
18. Andreasson, J. O., Shastry, S., Hancock, W. O. & Block, S. M. The mechanochemical cycle of mammalian kinesin-2 KIF3A/B under Load. *Curr. Biol.* **25**, 1166–1175 (2015).
19. Bensel, B. M. et al. The mechanochemistry of the kinesin-2 KIF3AC heterodimer is related to strain-dependent kinetic properties of KIF3A and KIF3C. *Proc. Natl Acad. Sci. USA* **117**, 15632–15641 (2020).
20. Brunnbauer, M. et al. Regulation of a heterodimeric kinesin-2 through an unprocessive motor domain that is turned processive by its partner. *Proc. Natl Acad. Sci. USA* **107**, 10460–10465 (2010).
21. Stepp, W. L., Merck, G., Mueller-Planitz, F. & Ökten, Z. Kinesin-2 motors adapt their stepping behavior for processive transport on axonemes and microtubules. *Embo Rep.* **18**, 1947–1956 (2017).

22. Rashid, D. J., Wedaman, K. P. & Scholey, J. M. Heterodimerization of the two motor subunits of the heterotrimeric kinesin, KRP85/95. *J. Mol. Biol.* **252**, 157–162 (1995).
23. De Marco, V., Burkhard, P., Le Bot, N., Vernos, I. & Hoenger, A. Analysis of heterodimer formation by Xklp3A/B, a newly cloned kinesin-II from Xenopus laevis. *EMBO J.* **20**, 3370–3379 (2001).
24. Vukajlovic, M., Dietz, H., Schliwa, M. & Okten, Z. How kinesin-2 forms a stalk. *Mol. Biol. Cell* **22**, 4279–4287 (2011).
25. Wedaman, K. P., Meyer, D. W., Rashid, D. J., Cole, D. G. & Scholey, J. M. Sequence and submolecular localization of the 115-kD accessory subunit of the heterotrimeric kinesin-II (KRP85/95) complex. *J. Cell Biol.* **132**, 371–380 (1996).
26. Yamazaki, H., Nakata, T., Okada, Y. & Hirokawa, N. Cloning and characterization of KAP3: a novel kinesin superfamily-associated protein of KIF3A/3B. *Proc. Natl Acad. Sci. USA* **93**, 8443–8448 (1996).
27. Garbouchian, A., Montgomery, A. C., Gilbert, S. P. & Bentley, M. KAP is the neuronal organelle adaptor for Kinesin-2 KIF3AB and KIF3AC. *Mol Biol Cell* **33**, https://doi.org/10.1091/mbc.E22-08-0336, (2022)
28. Doodhi, H. et al. KAP, the accessory subunit of kinesin-2, binds the predicted coiled-coil stalk of the motor subunits. *Biochemistry* **48**, 2248–2260 (2009).
29. Webb, S., Toropova, K., Mukhopadhyay, A. G., Nofal, S. D. & Roberts, A. J. Beta-hairpin mechanism of autoinhibition and activation in the kinesin-2 family. *bioRxiv*, https://doi.org/10.1101/2024.10.14.618219 (2014).
30. Snow, J. J. et al. Two anterograde intraflagellar transport motors cooperate to build sensory cilia on C. elegans neurons. *Nat. Cell Biol.* **6**, 1109–1113 (2004).
31. Chana, M. S., Tripet, B. P., Mant, C. T. & Hodges, R. Stability and specificity of heterodimer formation for the coiled-coil neck regions of the motor proteins Kif3A and Kif3B: the role of unstructured oppositely charged regions. *J. Pept. Res.* **65**, 209–220 (2005).
32. De Marco, V., De Marco, A., Goldie, K. N., Correia, J. J. & Hoenger, A. Dimerization properties of a Xenopus laevis kinesin-II carboxy-terminal stalk fragment. *Embo Rep.* **4**, 717–722 (2003).
33. Mertins, P. et al. Ischemia in tumors induces early and sustained phosphorylation changes in stress kinase pathways but does not affect global protein levels. *Mol. Cell Proteom.* **13**, 1690–1704 (2014).
34. Webb, S., Mukhopadhyay, A. G. & Roberts, A. J. Intraflagellar transport trains and motors: Insights from structure. *Semin Cell Dev. Biol.* **107**, 82–90 (2020).
35. Schorb, M., Haberbosch, I., Hagen, W. J. H., Schwab, Y. & Mastronarde, D. N. Software tools for automated transmission electron microscopy. *Nat. Methods* **16**, 471–477 (2019).
36. Punjani, A., Rubinstein, J. L., Fleet, D. J. & Brubaker, M. A. cryoSPARC: algorithms for rapid unsupervised cryo-EM structure determination. *Nat. Methods* **14**, 290–296 (2017).
37. Aiyer, S., Zhang, C., Baldwin, P. R. & Lyumkis, D. Evaluating Local and Directional Resolution of Cryo-EM Density Maps. *Methods Mol. Biol.* **2215**, 161–187 (2021).
38. Pettersen, E. F. et al. UCSF ChimeraX: Structure visualization for researchers, educators, and developers. *Protein Sci.* **30**, 70–82 (2021).
39. Wang, Q. S. et al. Upgrade of macromolecular crystallography beamline BL17U1 at SSRF. *Nucl. Sci. Tech.* **29**, https://doi.org/10.1007/s41365-018-0398-9 (2018).
40. Otwinowski, Z. & Minor, W. Processing of X-ray diffraction data collected in oscillation mode. *Methods Enzymol.* **276**, 307–326 (1997).
41. Varadi, M. et al. AlphaFold Protein Structure Database in 2024: providing structure coverage for over 214 million protein sequences. *Nucleic Acids Res.* **52**, D368–D375 (2024).
42. McCoy, A. J. Solving structures of protein complexes by molecular replacement with Phaser. *Acta Crystallogr. D. Biol. Crystallogr.* **63**, 32–41 (2007).
43. Emsley, P. & Cowtan, K. Coot: model-building tools for molecular graphics. *Acta Crystallogr. D. Biol. Crystallogr.* **60**, 2126–2132 (2004).
44. Adams, P. D. et al. PHENIX: a comprehensive Python-based system for macromolecular structure solution. *Acta Crystallogr. D. Biol. Crystallogr.* **66**, 213–221 (2010).
45. Xie, C. et al. Neurons dispose of hyperactive kinesin into glial cells for clearance. *EMBO J.* **43**, 2606–2635 (2024).

Acknowledgements

This work was supported by grants from the CAS Project for Young Scientists in Basic Research (YSBR-104 to W.F. and YSBR-075 to J.R.), the Chinese National Programs for Brain Science and Brain-like Intelligence Technology (2022ZD0205800 to J.R.), the Beijing Natural Science Foundation (5242021 to J.R.), and the Youth Innovation Promotion Association of CAS (to J.R.).

Author contributions

J.R., L.Z., and G.C. conducted experiments and participated in the design and interpretation of the experiments. G.O. provided the guidance for the IFT motility assay. W.F. designed all the experiments, interpreted the data and wrote the manuscript.

Competing interests

The authors declare no competing interests.

Additional information

Supplementary information The online version contains supplementary material available at https://doi.org/10.1038/s41467-025-62152-8.

Correspondence and requests for materials should be addressed to Wei Feng.

Peer review information *Nature Communications* thanks the anonymous reviewers for their contribution to the peer review of this work. A peer review file is available.